crystals

MDPI

Article

Successive Photocatalytic Degradation of Methylene Blue by ZnO, CuO and ZnO/CuO Synthesized from *Coriandrum sativum* Plant Extract via Green Synthesis Technique

Raja Abdul Basit [1], Zeeshan Abbasi [2], Muhammad Hafeez [1,*], Pervaiz Ahmad [3], Jahanzeb Khan [1,4], Mayeen Uddin Khandaker [5,6,*], Kholoud Saad Al-Mugren [7,*] and Awais Khalid [8]

1 Department of Chemistry, University of Azad Jammu and Kashmir, Muzaffarabad 13100, Pakistan
2 National Synchrotron Radiation Laboratory, University of Science and Technology of China, Hefei 230026, China
3 Department of Physics, University of Azad Jammu and Kashmir, Muzaffarabad 13100, Pakistan
4 Department of Chemistry, Mirpur University of Science and Technology, MUST, Mirpur 10250, Pakistan
5 Center for Applied Physics and Radiation Technologies, School of Engineering and Technology, Sunway University, Bandar Sunway 47500, Selangor, Malaysia
6 Department of General Educational Development, Faculty of Science and Information Technology, Daffodil International University, DIU Rd., Dhaka 1341, Bangladesh
7 Department of Physics, College of Science, Princess Nourah Bint Abdulrahman University, P.O. Box 84428, Riyadh 11671, Saudi Arabia
8 Department of Physics, Hazara University Mansehra, Mansehra 21300, Pakistan
* Correspondence: muhammadhafeezchemist@gmail.com (M.H.); mayeenk@sunway.edu.my (M.U.K.); ksalmogren@pnu.edu.sa (K.S.A.-M.)

Citation: Basit, R.A.; Abbasi, Z.; Hafeez, M.; Ahmad, P.; Khan, J.; Khandaker, M.U.; Al-Mugren, K.S.; Khalid, A. Successive Photocatalytic Degradation of Methylene Blue by ZnO, CuO and ZnO/CuO Synthesized from *Coriandrum sativum* Plant Extract via Green Synthesis Technique. *Crystals* **2023**, *13*, 281. https://doi.org/10.3390/cryst13020281

Academic Editors: Yashvir Singh, Nishant Kumar Singh and Erween Abd Rahim

Received: 6 January 2023
Revised: 27 January 2023
Accepted: 29 January 2023
Published: 7 February 2023

Abstract: In this study, successful synthesis of ZnO nanoparticles (NPs), CuO NPs, and ZnO/CuO nanocomposite through an eco-friendly method using *Corriandrum sativum* leaf extract as a capping agent is reported. Using XRD, FTIR, UV-Vis, and SEM techniques, the synthesized materials were characterized for structural analysis, functional groups identification, spectroscopic measurements, and morphological analysis. The percentage composition and purity of the samples were determined by using Energy Dispersive X-ray (EDX), which showed the synthesis of materials. Morphological analysis was done by Scanning Electron Microscopy (SEM) which reflected that the CuO NPs, ZnO NPs and ZnO/CuO nanocomposite were spherical, and the average size calculated by using Image J software was around 25 nm, 55 nm, and 11 nm, respectively. FTIR and UV-Vis analyses were used for synthetic confirmation through characteristic peaks of materials. The synthesized (ZnO, CuO, and CuO/ZnO) nanomaterials were evaluated for photocatalytic activity using methylene blue (MB) dye. Among all three photocatalysts, the composite showed maximum photodegradation compared to the other two materials. The present work could lead to a pathway for the decontamination of harmful dyes of wastewater released from different industries.

Keywords: zinc oxide; copper oxide; photocatalysis; visible light; green synthesis

1. Introduction

An advancement in the field of nanotechnology is the fabrication of NPs with environmentally friendly techniques, unique properties, and high efficiency for usage in a variety of fields [1]. For the fabrication of metal oxides, several chemical and physical procedures have been developed, including sol–gel, microwave irradiation, chemical vapor deposition, co-precipitation, wet impregnation, and mechanical alloying [2,3]. Among these approaches, the green method remains the most cost-effective, non-toxic, and ecologically friendly. Bio-synthesis, often known as green synthesis, has recently become a popular method for the synthesis of metal oxide nanostructures [4]. Chemical approaches can result in the accumulation of many hazardous compounds on the surface of NPs, which can have

negative consequences in catalytic applications [5,6]. This issue can be solved by using environmentally friendly methods to synthesize NPs [7]. Due to the promising applications of NPs in the field of science and technology, different forms of mixed metal oxides (MO) NPs received considerable attention. Prospective materials can have their chemical and physical properties improved by adding metals to an oxide matrix, which will lead to better performance in a range of applications. The metal in an oxide matrix system with matching band potentials may function as an isolated entity or have a variety of features as a result of the interactions between the metal and oxygen [8–10]. This might significantly improve the material's functionality and charge separation effectiveness [11]. It is critical to understand that the majority of single-phase mixed oxides display constituent oxide properties [12]. Antibacterial activity, photocatalysis, electrochemical sensors, and other applications have all made use of multiphase nanocomposite materials [13–17]. Metal oxide NPs such as CeO_2–MnO_x [18], CuO–ZnO [19], ZnO–NiO [20], ZnO–MgO [21], TiO_2–WO_3 [2], and Co_3O_4–ZnO [22] have been synthesized by several research groups by using various synthesis methods. Nonetheless, the green synthesis method has attracted huge attention as compared to other methods because of its simplicity, single-step nature, and less usage of energy features. Because of the excellent loading separation efficiency of metal oxide NPs, a great deal of attention has been paid to multiphase oxides [23–25]. Zinc oxide (ZnO) NPs, an exciting n-type semiconductor with direct bandgap, have piqued interest among metal oxides due to their appealing green qualities characteristics, exceptional stability, one-step synthesis process, and low-slung cost [26–28]. ZnO NPs have drawn interest due to their biological activities. Biological activity and quantitative evaluation of several metal oxide NPs against *Escherichia coli* and *Staphylococcus aureus* were both studied by J Sawai et al., who observed that ZnO NPs prevent the growth of bacteria by rupturing the cell membrane [29]. The nanotoxicity of ZnO NPs and their interaction with bacterial cells has been studied by several research groups [30–33]. Zinc oxide is used in a wide range of cosmetics and personal care products, including makeup, nail products, baby lotions, bath soaps, and foot powders. Zinc oxide is also used in skin protectants, such as diaper rash ointments and sunscreen products [16,34,35]. Zinc oxide is also used as a buffer layer in CIGS (Copper Indium Gallium Selenide) solar cells. Some current experiments focus on the effect of the thickness of ZnO on maximum power output for the cells [36–41]. Copper oxide (CuO) NPs are p-type semiconductor materials that have narrow band gaps and have been extensively used for a variety of applications because of their special environmentally friendly, anti-inflammatory, and anti-bacterial properties [10,16,31,42,43]. CuO has been extensively used for photoelectrochemical water reduction, photodegradation reactions, photovoltaic applications, solar hydrogen synthesis, and catalytic processes [16,31,44]. Numerous, natural, and synthetic dyes are widely utilized in the leather, textile, food, and plastic sectors. Dye-contaminated water has become a major pollutant from industries, posing a huge threat to aquatic/marine life. As a result, reducing the primary effluent colors before the harmful water enters water bodies is critical. Methyl red, one of the commonly used dyes, is released into the water reservoirs and causes water pollution [45–50]. CuO/ZnO, hierarchical metal oxide NPs, can be used as an amazingly effective photocatalyst for methyl red dye degradation. These metal oxide NPs are also employed in a variety of applications, including photovoltaic devices such as solar cells, sensing, and photocatalysis, due to their important properties, such as strong adsorption ability, extra sites for functional moieties, high porosity, etc. [51,52]. Biocides and disinfectants are also made with metal-oxide nanoparticles [53–56]. In this report, *Corriandrum sativum* plant is used for the green synthesis of ZnO, CuO, and ZnO/CuO nanocomposite. Alkaloids, glycosides, tannins, phenolic chemicals, flavonoids, and terpenoids are abundant in the plant, and can act as stabilizing and reducing agents according to previous studies [57]. Additionally, the above-mentioned plant is economic and abundant, and, to the best of our knowledge, the synthesis of ZnO, CuO NPs, and ZnO/CuO nanocomposite has not been done using *Corriandrum sativum* leaf extract until now. The synthesized ZnO, CuO

NPs, and ZnO/CuO nanocomposite were investigated as a potential photocatalyst against methylene blue dye.

2. Materials and Methods

2.1. Materials

To make 0.1 M solution of copper sulphate salt, 6.2 g of copper sulphate (II) ($CuSO_4.5H_2O$) (99.00 % pure, Guangdong, Guanghua chemical factory Co. Ltd., Shantou, Guangdong, China) was dissolved in 250 mL of distilled water. 0.1 M solution of zinc acetate (99.99% pure, acquired from Duksan Pure Chemicals Co., Ltd., Ansan, Republic of Korea) was made by dissolving 5.48 g of $Zn(CH_3CO_2)_2$ in 250 mL of distilled water. For later usage, both prepared solutions were safely stored in screw-top bottles that were covered with aluminum foil and kept at room temperature in a dark cupboard. Sodium hydroxide (NaOH) was purchased from Alfa Aesar. The green *Corriandrum sativum* leaves were collected from the local market (Muzaffarabad, Pakistan). The collected green leaves underwent a thorough deionized water wash before being allowed to air dry for four days at room temperature. To make the extract, 50 g of leaves were taken into 1000 mL (distilled water) and boiled at 80 °C for 3 h until the aqueous part turned a brown color. The extract was filtered by using the Whatmann filter paper. The filtrate was poured into a measuring flask and stored in the refrigerator for further use. Without additional purification, all substances were utilized exactly as received.

2.2. Synthesis of ZnO

Green synthesis of ZnO NPs was conducted by adding 20 mL of *Coriandrum sativum* plant extract into 50 mL of salt solution and kept on constant stirring using a thermostat at 700 rpm and 80 °C. Sodium hydroxide was added after every 20 min to maintain the pH at 13. The reaction was conducted until the bright peach-colored precipitates appeared. Precipitates were allowed to settle down and were washed with distilled water 3–4 times. Precipitates were dried out in an oven at 100 °C for an hour and converted into fine powder with the help of a mortar and pestle. The powder was washed again with distilled water 3–4 times. Calcination was done at 350 °C for 3 h and converted into a fine and homogeneous powder with the help of a mortar and pestle.

2.3. Synthesis of CuO

Synthesis of CuO NPs was done by adding 20 mL of *Coriandrum sativum* plant extract into 50 mL of salt solution with constant stirring of 900 rpm at 90 °C. Sodium hydroxide was added after every 20 min to maintain the pH at 13. The reaction was conducted until the black-colored precipitates appeared. Precipitates were allowed to settle down and washed with distilled water 3–4 times. Precipitates were dried out in an oven at 100 °C and were converted into a fine powder with the help of a mortar and pestle. The powder was washed again with distilled water 3–4 times. Calcination was done at 350 °C for 3 h and converted into a fine and homogeneous powder with the help of a mortar and pestle.

2.4. Synthesis of ZnO/CuO Nanocomposite

ZnO/CuO nanocomposite was synthesized by taking a 50 mL solution of both zinc sulphate and copper sulphate in the 500 mL flask. Following that, 40 mL of *Corriandrum sativum* plant extract was added and reactions were kept on constant stirring at 700 rpm and 80 °C for 3 h. Reactions were carried out until precipitates appeared. The precipitate formation was the indication of ZnO/CuO nanocomposite synthesis. Precipitates were allowed to settle down and washed with distilled water 3 to 4 times. Precipitates were dried in an oven at 100 °C and converted into a fine powder with the help of a mortar and pestle. The powder was washed again with distilled water 3–4 times. Calcination was done at 350 °C for 3 h and converted into very fine and homogeneous powder with the help of a mortar and pestle.

2.5. Photocatalytic Activity

The photocatalytic activity of the ZnO, CuO, and ZnO/CuO was evaluated by photodegradation of an aqueous MB textile dye. The experiment was carried out in an open atmosphere under the UV-Vis light coming from the Sun. The catalyst material used in the catalytic tests included 5 mg each of ZnO, CuO, and ZnO/CuO NPs under continual stirring in a 50 mL solution of MB (15×10^{-6} M). Following that, 4 mL aliquots were taken from each reaction mixture at predetermined intervals (10 min), centrifuged, and the decrease in absorbance values was recorded using spectrophotometry.

2.6. Characterization of ZnO, CuO and ZnO/CuO Nanocomposite

UV spectroscopic analysis was performed using a Shimadzu UV-1700 UV spectrophotometer outfitted with tungsten and deuterium lamps. The light source's variable wavelength was set to 340.8 nm, and the spectrophotometer's wavelength range was 190–1100 nm with a 1 nm width. For spectral investigations, a quartz crystal with a length of 10 mm was employed. In this publication, UV-Vis spectra of ZnO NPs, CuO NPs, and ZnO/CuO nanocomposite were studied. The size and shape of produced NPs and nanocomposite were characterized using the Nova Nano SEM, which has a 20–200,000× magnification range and a resolution of up to 1 nm. EDX analysis of powder samples was done by FEI NOVA nano SEM 450 equipped with an Oxford EDX detector. The X-ray diffraction pattern of ZnO NPs, CuO NPS, and ZnO/CuO nanocomposite was recorded, with Bruker D8 Advance instrument having (Cu) K_α radiation of wavelength λ = 1.5406 Å. The 2θ viewing range was 20°–70° and the generator setting was 30 mA at 40 kV. A customized high-temperature Box Muffle Furnace (KSL-1800X-KA-UL) by MTI Corporation was used for the calcination of samples. Using the Shimadzu FTIR-8400S Spectrometer, FTIR investigations were carried out. The peak-to-peak S/N ratio of the spectrometer was 20,000:1, and its resolution was 0.85 cm^{-1}. ZnO, CuO, and ZnO/CuO nanocomposite transmittance were tested in the 500–4000 cm^{-1} range. Different functional groups in ZnO, CuO, and ZnO/CuO Nanocomposite were identified using FT-IR.

3. Results and Discussion

3.1. ZnO NPs

ZnO nanoparticles were characterized by FT-IR spectroscopy, UV-Vis spectroscopy, X-ray diffraction analysis (XRD), and scanning electron microscopy studies (Figure 1). FT-IR spectrum of ZnO NPs (Figure 1a) shows different peaks in the range of 4000–400 cm^{-1}. The main absorption band at 3455 cm^{-1} is assigned to the O–H group stretching vibrations [58]. The range between 1700–1545.02 cm^{-1} represents the stretching modes of C=O and Zn-O bonds [59]. Peaks in the range of 1000–1200 cm^{-1} are attributed to M-O bond formation in the presence of NaOH [60]. The peak at 617.9 cm^{-1} represented Zn-O stretching vibrations which was the confirmation of the synthesis of ZnO NPs. UV–Vis spectrum (Figure 1b) of ZnO NPs dispersed in water showed the absorption band at 372 nm. In the spectrum, the band at 372 nm was due to surface plasmon absorption of metal oxide. The absorption band at 372 nm confirmed the zinc oxide NPs formation [61]. Figure 1c shows the XRD spectrum of ZnO NPs. The XRD was taken at a scanning step of 0.020°, in 2θ range from 20° to 70° with mono-chromatic Cu-Kα radiation (λ = 0.51418 nm). The diffraction patterns were analyzed from the standard diffraction files of ZnO (Ref. Code 00-001-1136). The characteristic peaks at 2θ values, 31.85°, 36.35°, 47.55°, 56.65°, 62.95°, 66.35°, 68.05°, 69.15°, 72.6, and 79.95°, corresponded to the (100), (002), (101), (102), (110), (103), (200), (201), (004), (202), and (104) Miller indices, respectively, that match to the standard structural values. Using the X'Pert HighScore software, it was found that the D-spacing and density of crystallite from the XRD spectrum were at 3.56 and 5.66 gcm^{-3}, respectively [62].

Morphology and sizes of ZnO NPs were analyzed at the magnifications of 500 nm, with the help of Nova Nano SEM (Figure 1d). It showed various irregular shapes of ZnO NPs. At some points, NPs were combined to form agglomeration and cavities were also seen at various points. The average crystallite size of ZnO NPs calculated from the XRD

pattern using the Sherrer equation was 54.7 nm, and the SEM image using Image J software was found to be averaged at 55 nm. The surface was smooth with clear boundaries, except for agglomerated points [63]. EDX analysis (Figure 1e) showed that the powder sample consisted of Zn, O, C, and Ca constituents with weight percentages of 73.21, 21.73, 4.29, and 0.77, respectively. EDX confirmed the signal characteristic of Zn and O with a very small negligible amount of C and Ca in the sample. This spectrum correctly identified the presence of Zn and O. All the above-obtained results confirmed the synthesis of ZnO NPs [28].

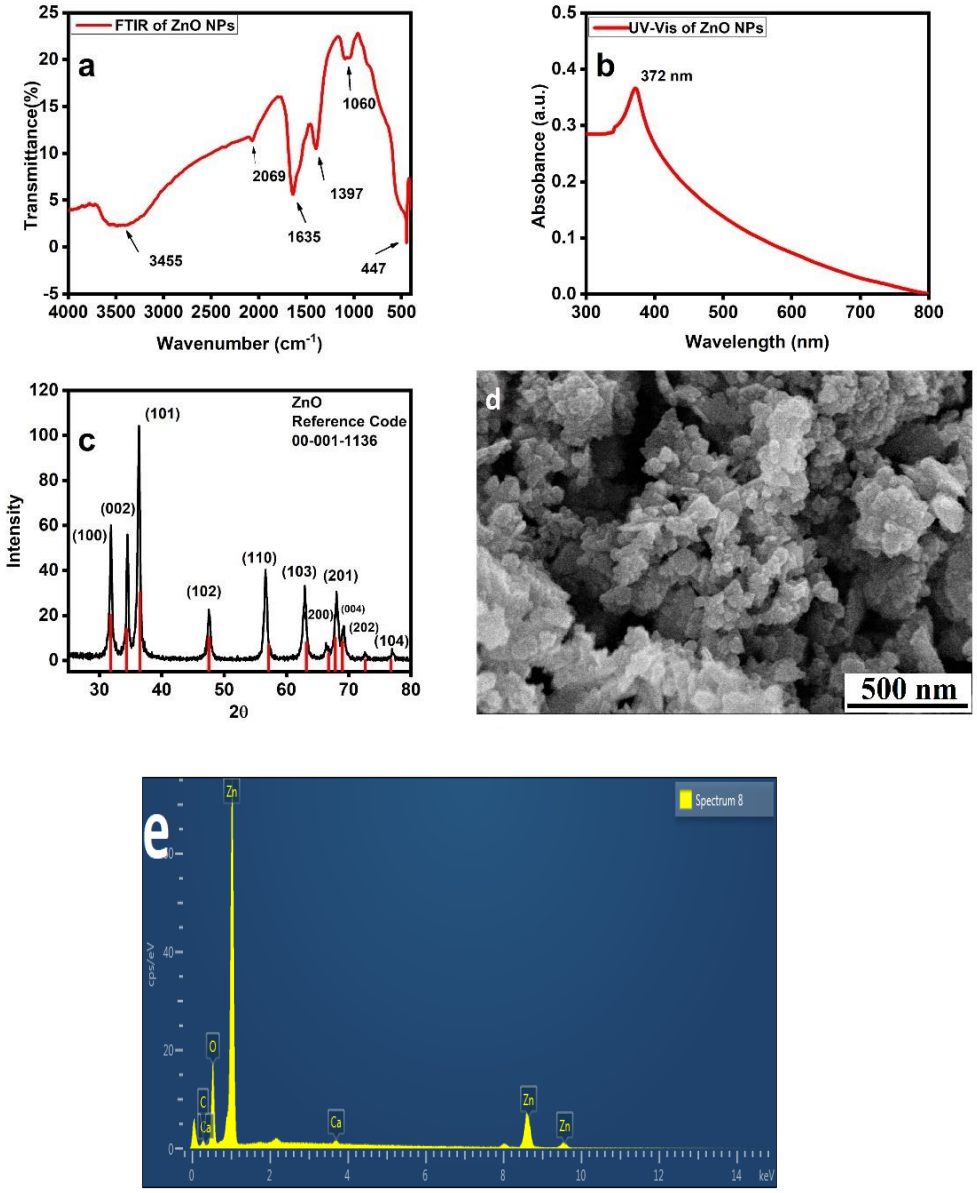

Figure 1. (**a**) FT-IR spectrum of ZnO NPs, (**b**) UV absorption spectrum of ZnO NPs, (**c**) XRD pattern of ZnO NPs, (**d**) HRSEM image of ZnO NPs, (**e**) EDX image of ZnO NPs.

3.2. CuO NPs

Figure 2 shows various characterizations such as FT-IR spectroscopy, UV-Vis spectroscopy, X-ray Diffraction analysis (XRD), and scanning electron microscope images of CuO nanoparticles. Figure 2a shows the FT-IR spectrum of CuO NPs with different peaks in the range of 4000–400 cm^{-1}. The band between 3615.3–3286.0 cm^{-1} was attributed to the stretching vibrations of the hydrogen-bonded O-H group [58]. The peak at 1627 cm^{-1} represented the stretching vibrations of C=O [64]. The presence of O-H with the formation of Cu-O bond was represented at 1382 cm^{-1} [60]. Peaks in the range of 522–1200 cm^{-1} were

attributed to Cu bond formation in the presence of NaOH. Strong sharp peaks were seen at 694.4 cm^{-1} and 786 cm^{-1} that were attributed to CuO [60]. Cu-O stretching vibration was observed at 522 cm^{-1}, which matched the stretching mode of vibration [60,64]. The UV-Vis spectra of the CuO NPs are shown in Figure 2b, with water absorption occurring at 386 nm. The metal oxide's surface plasmon absorption resulted in the absorption at 386 nm in the spectrum. In metal oxide nanoparticles (NPs), surface plasmon absorption is linked to the collective oscillation of free conduction band electrons that are activated by electromagnetic radiation. When the wavelength of the incident light is bigger than the particle's diameter, this form of resonance takes place. CuO NPs were formed, as shown by a surface plasmon absorption band with a peak at 386 nm [65]. Figure 2c shows the XRD spectrum of CuO nanoparticles. The diffraction patterns were analyzed from the standard diffraction files of CuO (Ref. Code 00-001-1117) giving the characteristic peaks at 2θ at about 35.65°, 38.9°, 48.9°, 53.9°, 58.35°, 61.7°, 66.2°, 68.1°, 72.15°, and 75.35°, corresponding to the (−111), (111), (−202), (020), (202), (−113), (022), (220), (311), and (004) Miller indices, respectively, that match the standard values with the D-spacing value of 3.84 A^0 and density of crystallite 6.10 gcm^{-3} [62].

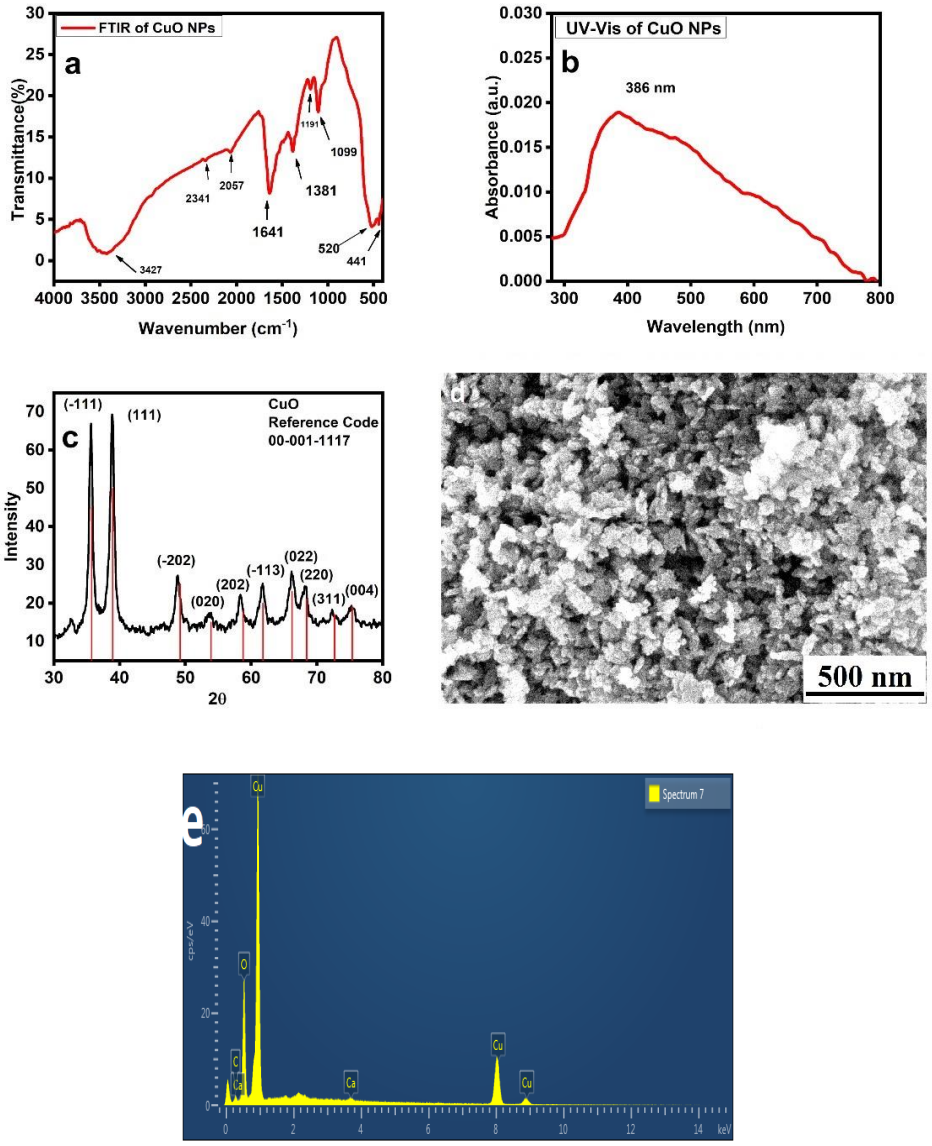

Figure 2. (**a**) FT-IR spectrum of CuO NPs, (**b**) UV absorption spectrum of CuO NPs, (**c**) XRD pattern of CuO NPs, (**d**) HRSEM image of CuO NPs, (**e**) EDX image of CuO NPs.

The SEM image of CuO NPs is shown in Figure 2d. SEM images at the magnification of 200 nm were employed to give the morphology of the CuO NPs, where the majority of the CuO NPs possess spherical shapes [29]. The average crystallite size of CuO NPs calculated from the XRD pattern using the Sherrer equation was 23 nm, and it was found to be 25 nm from SEM using image j software. The surface of nanoparticles is smooth with clear boundaries. Analysis by Energy dispersive X-ray spectroscopy (EDX) of CuO is given in (Figure 2e), which confirmed that the prepared powder sample contained constituents, namely Cu, O, C, and Ca, with weight percentages of 72.38, 23.59, 3.58, and 0.45%, respectively. The amount of calcium and carbon is negligible. Both calcium and carbon come from leaf extracts. Carbon content could be removed by hot water washing.

3.3. ZnO/CuO Nanocomposites

Figure 3 shows various characterizations such as FT-IR spectroscopy, UV-Vis spectroscopy, X-Ray diffraction analysis (XRD), and scanning electron microscope images of CuO NPs. Figure 3a represents the FT-IR spectrum of ZnO/CuO obtained by IR spectrophotometer in terms of % transmittance. The broad band at 3652.8–3170.9 cm^{-1} represents the O-H bond [58]. The peak at 1645.19 cm^{-1} is attributed to stretching vibrations of C=O [64]. The peak at 1500.47 cm^{-1} is attributed to bending vibrations of the H_2O molecule [66]. Peaks in the range of 1000–1200 cm^{-1} are attributed to M-O bond formation in the presence of NaOH [60]. The stretching mode of the Zn-O bond is given at 495 cm^{-1}. Zn-O stretching vibrations are shifted to 495 cm^{-1} from 485 cm^{-1} with the addition of Cu-O Peak at 485 cm^{-1}, which is attributed to the stretching mode by the combination of Zn-O and Cu-O [66]. Synthesized ZnO/CuO NPs were subjected to UV–Visible spectrophotometer analysis which confirmed the formation of particles in the initial stage. The solid greyish, black-colored samples of ZnO/CuO nanocomposite synthesized using *Corriandrum sativum* were subjected to a scan UV-Spectrophotometer in the range of 200–1000 nm. Figure 3b shows the UV–Vis spectra of the as-synthesized ZnO/CuO nanocomposite dispersed in water exhibiting the maximum absorption peaks at about 374 nm and 438 nm, respectively. In the spectrum, the peaks at 374 nm and 438 nm confirmed the formation of nanocomposite [3]. The diffraction patterns were analyzed from the standard diffraction files of ZnO (Ref. Code 00-001-1136) and CuO (Ref. Code 00-001-1117). The characteristic peak at 2θ at about 31.85°, 34.6°, 35.8°, 36.4°, 38.85°, 47.6°, 48.75°, 53.8°, 56.75°, 58.35°, 61.85°, 63.05°, 66.7°, 68.45°, 69°.15, 72.75°, 72.7°, 75.25°, 76.8°, and 79.95° correspond to the (100), (002), (−111), (101), (111), (102), (−202), (020), (110), (202), (−113), (110), (022), (200), (220), (112), (201), (311), (004), and (004) Miller indices, respectively, that match to the standard values.

Figure 3d illustrates the morphology and size of the ZnO/CuO nanocomposite that was analyzed at high magnification (500 nm). Elongated and irregularly shaped small particles are seen on the surface with smooth unclear boundaries. At some points, nanocomposites are seen to agglomerate and form chunks and cavities. In the case of the nanocomposite, the average crystallite size calculated from the XRD pattern using the Sherrer equation was 11.3 nm, and it was found to be 11 nm from SEM using image j software. The results of Energy Dispersive X-ray Spectroscopy are given in (Figure 3e), which show the presence of Zn, Cu, O, C, Si, S, and C constituents with weight percentages of 36.87, 27.65, 21.32, 12.92, 0.34, 0.34, and 0.56%, respectively. By the presence of Zn, Cu, and O, the formation of ZnO/CuO nanocomposite could be predicted. The sample is synthesized from the green method by using plant extracts, so the presence of C could be justified. A minute amount of calcium, sulfur, and silicon is also present. Calcium and sulfur come from leaf extracts, while silicon is due to calcination holder.

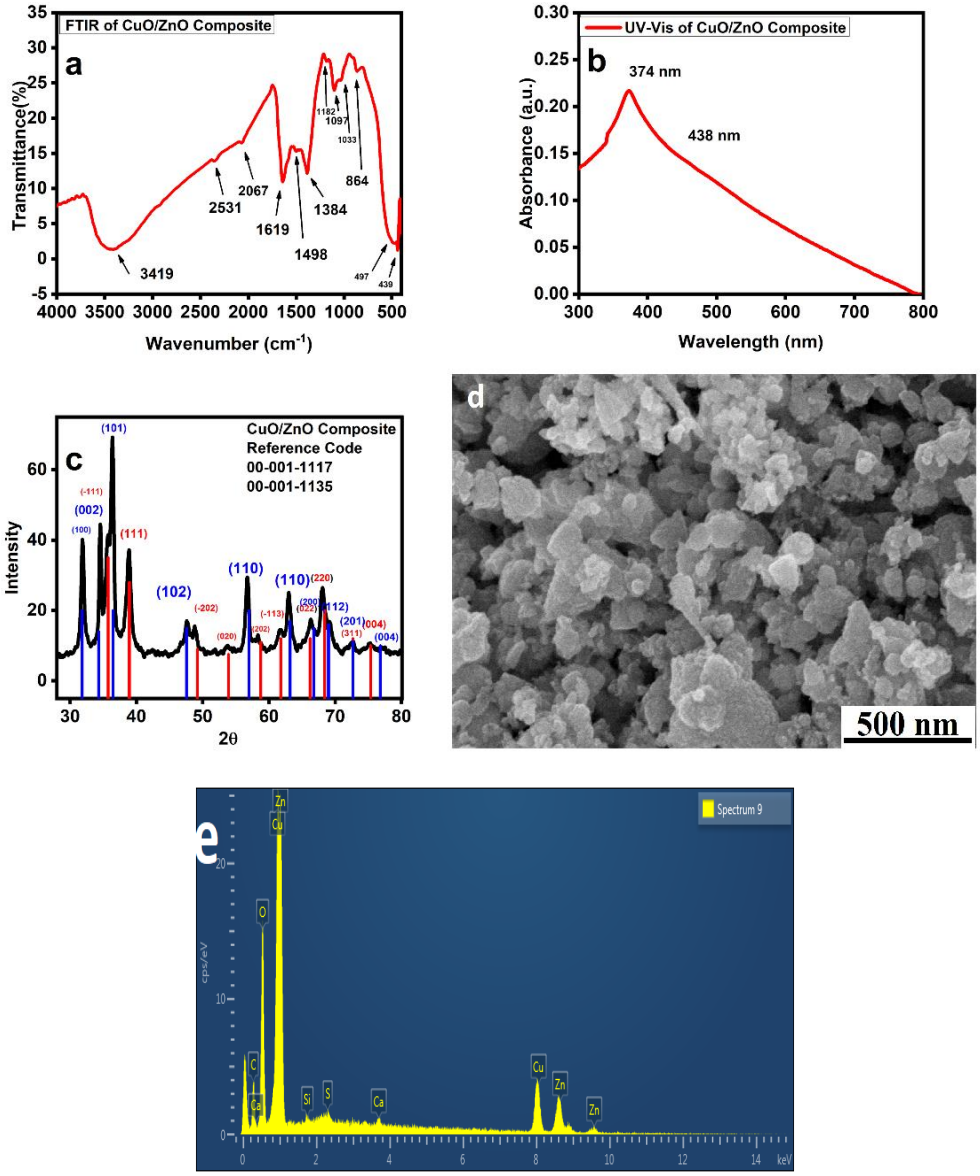

Figure 3. (**a**) FT-IR spectrum of ZnO/CuO, (**b**) UV absorption spectrum of ZnO/CuO, (**c**) XRD pattern of ZnO/CuO, (**d**) HRSEM image of ZnO/CuO, (**e**) EDX image of ZnO/CuO nanocomposite.

3.4. Photocatalytic Activity

Barzegar et al. reported methylene blue (MB) dye degradation photo catalytically by CdS nanoparticles when exposed to UV light [67]. In the present study, the comparative photocatalytic activity of ZnO, CuO, and ZnO/CuO was done using MB dye. The photo decolorization of the MB dye, when exposed to sunlight, served as a measurement of the dye's degradation. The absorbance spectra for the photocatalysts ZnO, CuO, and ZnO/CuO at a concentration of 5 mg are shown in Figure 4a–c, respectively. The photo-decolorization process makes it abundantly evident that the absorbance gradually lowers with rising exposure duration. It is also observed that the photocatalytic activity of the ZnO/CuO catalyst is higher as compared to CuO and ZnO NPs. In addition, the close intercalation of CuO and ZnO NPs in the ZnO/CuO nanocomposite should be essential in boosting photo reactivity [68]. ZnO/CuO NPs are generally tightly packed, which speeds up electron flow between the surfaces and prevents photogenerated electrons and holes from recombining. Superoxide radical anions, photogenerated holes, and hydroxyl radicals all play active roles in the photocatalytic degradation of MB dye solution [31,68]. According

to findings from the literature, OH and holes play a significant role in the photocatalytic destruction of organic pollutants by ZnO and CuO, and ZnO/CuO NPs under UV light.

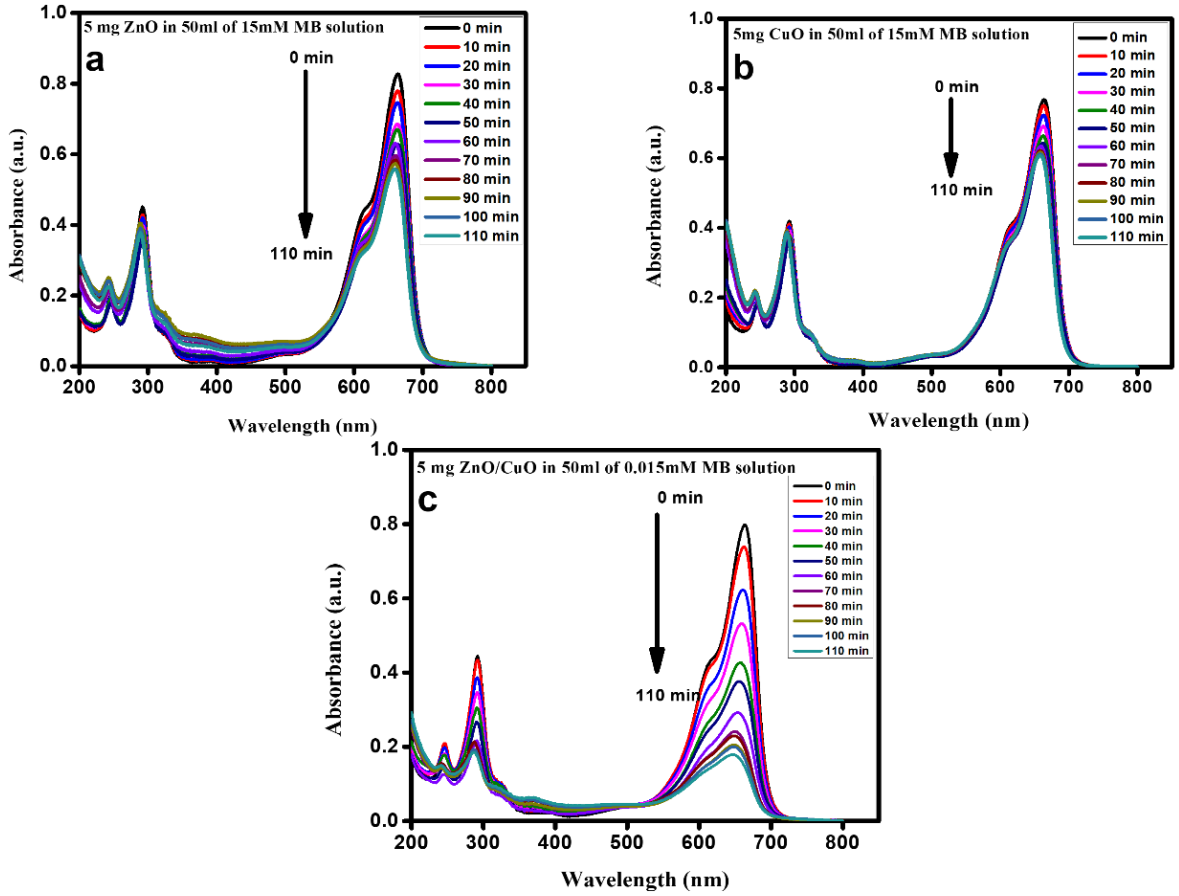

Figure 4. (**a**–**c**) Absorbance spectra of a 50 mL solution of Methylene Blue [5×10^{-6} M] dye containing 5 mg each of ZnO, CuO, and ZnO/CuO nanocomposite powder at various times points.

3.5. Comparison of Photocatalytic Degradation

The photocatalytic degradation process makes it abundantly evident that the absorbance steadily lowers with increasing exposure time [35]. The photodegradation and photocatalytic activity of different catalysts for the photodegradation of MB dye under irradiation are displayed in Figure 5a. This demonstrates that during the irradiation period, ZnO/CuO's photocatalytic performance was more intense than that of the other two catalysts. Figure 5a shows the comparative photodegradation of as-synthesized samples, namely ZnO, CuO, and ZnO/CuO in MB under UV irradiation. From this comparative study, it was observed that ZnO/CuO nanocomposite exhibited better photodegradation performance than ZnO and CuO NPs. The linear fitting of the absorbance spectra of the MB dye solution containing 5 mg of ZnO, CuO NPs, and ZnO/CuO nanocomposite is shown in Figure 5b. The highest photocatalytic activity was attained using a ZnO/CuO nanocomposite that had a concentration of 5 mg. Moreover, the nanocomposite outperforms the other two catalysts in terms of degrading efficiency. The degradation efficiency can be calculated using Equation (1).

$$\eta = \frac{C_0 - C}{C_0} \times 100 = \frac{A_0 - A}{A_0} \times 100 \quad (1)$$

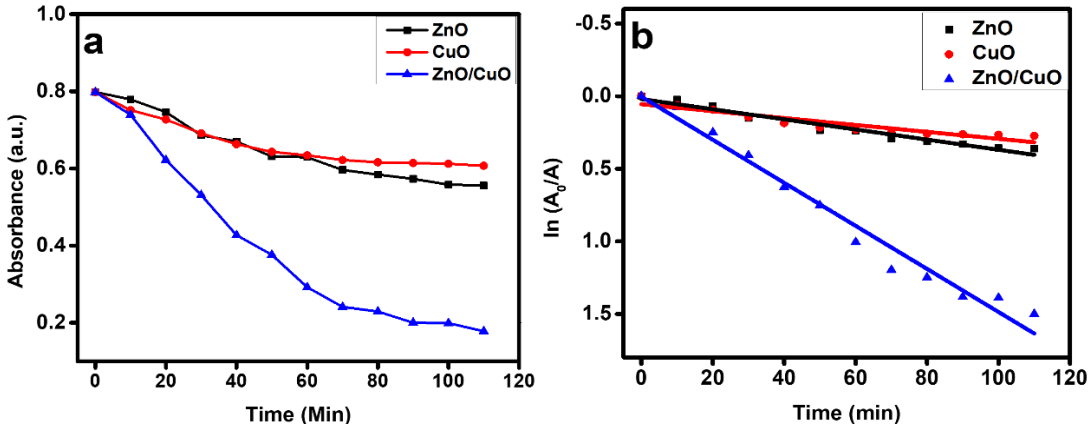

Figure 5. (**a**) Variation of absorbance measured at 341 nm with sunlight exposure time, (**b**) the linear fitting for the absorbance spectra of MB dye solution containing 5 mg of ZnO, CuO, and ZnO/CuO nanocomposite.

The initial dye concentration in this case is C_0, and the matching absorbance value is A_0 [69]. Following irradiation, the dye concentration is C, and the matching absorbance value is A [30–32].

The plot of $\ln(A_0/A)$ versus irradiation time for all samples is shown in Figure 5b.

According to first-order kinetics, the degradation rate constant (k) is determined from the straight-line graph using linear fitting: $\ln(A_0/A) = kt$ [70,71].

Table 1 shows the calculated k values and accompanying linear regression coefficients (R^2).

Table 1. Photocatalytic reaction parameters of ZnO, CuO, and ZnO/CuO nanocomposite.

Sr. No	Type of Catalyst	Rate Constant (k) min^{-1}	R2
1	ZnO/CuO	0.0148	0.9749
2	CuO	0.0025	0.9568
3	ZnO	0.0036	0.9696

The ZnO/CuO nanocomposite obviously exhibits improved photocatalytic performance, according to the values of k and R^2. The performance of the photocatalyst is enhanced by the existence of more efficient ions (species), having a higher surface area and active sites. The conclusion from the foregoing explanation is that ZnO/CuO has significantly better photocatalytic activity than the other two catalysts.

4. Conclusions

It is concluded that the use of plant extract for the synthesis of NPs and nanocomposite proved to be one of the most effective, fast, affordable, and non-toxic methods. The bioactive components of plant extract play a vital role in the synthesis of NPs and nanocomposites that function as stabilizing or capping agents. *Corriandrum sativum* was used for the synthesis of CuO and ZnO nanoparticles and ZnO/CuO nanocomposite to degrade organic dye by photocatalysis. All the physiochemical properties of the samples were examined through different characterization techniques such as EDX, SEM, and FTIR. The EDX results of CuO NPs revealed that the given sample contained Cu (72.38%) and O (23.59%), respectively. SEM showed that CuO NPs were found to have a spherical shape with an average size of 25 nm, and FTIR indicates a stretching band at 522 cm^{-1} for CuO that confirmed the formation of CuO NPs. The EDX results of ZnO confirmed that the given sample contained ZnO (73.21%) and O (21.73%), respectively. SEM results showed an irregular shape of ZnO NPs with an average size of 55 nm, and FTIR confirmed the synthesis of ZnO NPs with the band at 372 cm^{-1}. Percent composition of Zn, Cu, and O in ZnO/CuO nanocomposite was found to be 36.87%, 27.65%, and 21.32%, respectively, by

EDX analysis. Irregular and elongated shapes with an average of 11 nm were observed by SEM, and the peak at 485 cm^{-1} by FTIR confirmed the synthesis of ZnO/CuO nanocomposite. The average crystallite size of CuO, ZnO, and ZnO/ZnO was 25 nm, 55 nm, and 11 nm, respectively. Among all three photocatalysts, the composite showed maximum photodegradation. Because of the ease in the synthesis and biocompatibility of the materials, these materials can be used for the photodegradation of many other hazardous organic compounds present in both industrial and domestic water resources.

Author Contributions: Conceptualization, R.A.B., Z.A., M.H. and P.A.; Data curation, R.A.B., Z.A., M.H., A.K. and P.A.; Formal analysis, R.A.B., Z.A. and M.H.; Funding acquisition, M.U.K. and K.S.A.-M..; Investigation, R.A.B., Z.A., M.H. and A.K.; Methodology, Z.A., M.H. and P.A.; Project administration, M.U.K. and M.H.; Resources, P.A., M.U.K. and K.S.A.-M.; Supervision, M.H; Validation, K.S.A.-M., P.A., M.U.K. and J.K.; Visualization, A.K., J.K. and K.S.A.-M.; Writing—original draft, R.A.B., Z.A., M.H., P.A., J.K. and A.K.; Writing—review & editing, R.A.B., Z.A., M.H., A.K., P.A. and J.K. All authors have read and agreed to the published version of the manuscript.

Funding: Princess Nourah bint AbdulRahman University Researchers Supporting Project number (PNURSP2023R10), Princess Nourah bint AbdulRahman University, Riyadh, Saudi Arabia.

Data Availability Statement: All the data are available within the manuscript.

Conflicts of Interest: The authors declare no conflict of interest.

References

1. Palmero, P. Structural ceramic nanocomposites: A review of properties and powders' synthesis methods. *Nanomaterials* **2015**, *5*, 656–696. [CrossRef]
2. Su, C. Environmental implications and applications of engineered nanoscale magnetite and its hybrid nanocomposites: A review of recent literature. *J. Hazard. Mater.* **2017**, *322*, 48–84. [CrossRef]
3. Mohammadi-Aloucheh, R.; Habibi-Yangjeh, A.; Bayrami, A.; Latifi-Navid, S.; Asadi, A. Green synthesis of ZnO and ZnO/CuO nanocomposites in Mentha longifolia leaf extract: Characterization and their application as anti-bacterial agents. *J. Mater. Sci. Mater. Electron.* **2018**, *29*, 13596–13605. [CrossRef]
4. Vibitha, B.V.; Anitha, B.; Tharayil, N.J. Green synthesis of ZnO: CuO nanocomposites by Aloe Barbadansis leaf extract: Structure and photo catalytic properties. In Proceedings of the AIP Conference Proceedings, AIP Publishing LLC, 2020; p. 020031.
5. Parashar, U.K.; Saxena, P.S.; Srivastava, A. Bioinspired synthesis of silver nanoparticles. *Dig. J. Nanomater. Biostructures (DJNB)* **2009**, *4*, 159–166.
6. Khalid, A.; Ahmad, P.; Khan, A.; Muhammad, S.; Khandaker, M.U.; Alam, M.; Asim, M.; Din, I.U.; Chaudhary, R.G.; Kumar, D.J.B.C.; et al. Effect of Cu Doping on ZnO Nanoparticles as a Photocatalyst for the Removal of Organic Wastewater. *Bioinorg. Chem. Appl.* **2022**, *2022*, 9459886. [CrossRef] [PubMed]
7. Begum, N.A.; Mondal, S.; Basu, S.; Laskar, R.A.; Mandal, D. Biogenic synthesis of Au and Ag nanoparticles using aqueous solutions of Black Tea leaf extracts. *Colloids Surf. B Biointerfaces* **2009**, *71*, 113–118. [CrossRef] [PubMed]
8. Rodriguez, J.A.; Wang, X.; Hanson, J.C.; Liu, G. The behavior of mixed-metal oxides: Structural and electronic properties of $Ce_{1-x}Ca_xO_2$ and $Ce_{1-x}Ca_xO_{2-x}$. *J. Chem. Phys.* **2003**, *119*, 5659–5669. [CrossRef]
9. Ahmed, S.; Jiang, X.; Wang, C.; Kalsoom, U.e.; Wang, B.; Khan, J.; Muhammad, Y.; Duan, Y.; Zhu, H.; Ren, X.; et al. An Insightful Picture of Nonlinear Photonics in 2D Materials and their Applications: Recent Advances and Future Prospects. *Adv. Opt. Mater.* **2021**, *9*, 2001671. [CrossRef]
10. Abbasi, Z.; Saeed, W.; Shah, S.M.; Shahzad, S.A.; Bilal, M.; Khan, A.F.; Shaikh, A.J. Binding efficiency of functional groups towards noble metal surfaces using graphene oxide–metal nanoparticle hybrids. *Colloids Surf. A Physicochem. Eng. Asp.* **2021**, *611*, 125858. [CrossRef]
11. Wang, Y.; Cai, L.; Li, Y.; Tang, Y.; Xie, C. Structural and photoelectrocatalytic characteristic of ZnO/ZnWO4/WO3 nanocomposites with double heterojunctions. *Phys. E: Low-Dimens. Syst. Nanostructures* **2010**, *43*, 503–509. [CrossRef]
12. Arandiyan, H.; Parvari, M. Studies on mixed metal oxides solid solutions as heterogeneous catalysts. *Braz. J. Chem. Eng.* **2009**, *26*, 63–74. [CrossRef]
13. Ong, C.B.; Ng, L.Y.; Mohammad, A.W. A review of ZnO nanoparticles as solar photocatalysts: Synthesis, mechanisms and applications. *Renew. Sustain. Energy Rev.* **2018**, *81*, 536–551. [CrossRef]
14. Kumar, R.; Umar, A.; Kumar, G.; Nalwa, H.S. Antimicrobial properties of ZnO nanomaterials: A review. *Ceram. Int.* **2017**, *43*, 3940–3961. [CrossRef]
15. Qi, K.; Cheng, B.; Yu, J.; Ho, W. Review on the improvement of the photocatalytic and antibacterial activities of ZnO. *J. Alloy. Compd.* **2017**, *727*, 792–820. [CrossRef]
16. Hafeez, M.; Arshad, R.; Khan, J.; Akram, B.; Ahmad, M.N.; Hameed, M.U.; Haq, S. Populus ciliata mediated synthesis of copper oxide nanoparticles for potential biological applications. *Mater. Res. Express* **2019**, *6*, 055043. [CrossRef]

17. Ahmad, K.; Khan, B.A.; Akram, B.; Khan, J.; Mahmood, R.; Roy, S.K. Theoretical investigations on copper catalyzed C N cross-coupling reaction between aryl chlorides and amines. *Comput. Theor. Chem.* **2018**, *1134*, 1–7. [CrossRef]
18. Hussain, I.; Singh, N.; Singh, A.; Singh, H.; Singh, S. Green synthesis of nanoparticles and its potential application. *Biotechnol. Lett.* **2016**, *38*, 545–560. [CrossRef] [PubMed]
19. Singh, J.; Kaur, G.; Rawat, M. A brief review on synthesis and characterization of copper oxide nanoparticles and its applications. *J. Bioelectron. Nanotechnol.* **2016**, *1*, 9.
20. Peralta-Videa, J.R.; Huang, Y.; Parsons, J.G.; Zhao, L.; Lopez-Moreno, L.; Hernandez-Viezcas, J.A.; Gardea-Torresdey, J.L. Plant-based green synthesis of metallic nanoparticles: Scientific curiosity or a realistic alternative to chemical synthesis? *Nanotechnol. Environ. Eng.* **2016**, *1*, 1–29. [CrossRef]
21. Dey, A. Semiconductor metal oxide gas sensors: A review. *Mater. Sci. Eng. B* **2018**, *229*, 206–217. [CrossRef]
22. Boro, B.; Gogoi, B.; Rajbongshi, B.; Ramchiary, A. Nano-structured TiO2/ZnO nanocomposite for dye-sensitized solar cells application: A review. *Renew. Sustain. Energy Rev.* **2018**, *81*, 2264–2270. [CrossRef]
23. Sundar, L.S.; Sharma, K.; Singh, M.K.; Sousa, A. Hybrid nanofluids preparation, thermal properties, heat transfer and friction factor–a review. *Renew. Sustain. Energy Rev.* **2017**, *68*, 185–198. [CrossRef]
24. Khalid, A.; Ahmad, P.; Muhammad, S.; Khan, A.; Khandaker, M.U.; Alam, M.M.; Asim, M.; Din, I.U.; Iqbal, J.; Rehman, I.U. Synthesis of Boron-Doped Zinc Oxide Nanosheets by Using Phyllanthus Emblica Leaf Extract: A Sustainable Environmental Applications. *Front. Chem.* **2022**, *10*, 930620. [CrossRef]
25. Saeed, W.; Abbasi, Z.; Bilal, M.; Shah, S.H.; Waseem, A.; Shaikh, A.J. Interactive behavior of graphene quantum dots towards noble metal surfaces. *Phys. E Low-Dimens. Syst. Nanostructures* **2023**, *147*, 115596. [CrossRef]
26. Gawande, M.B.; Shelke, S.N.; Zboril, R.; Varma, R.S. Microwave-assisted chemistry: Synthetic applications for rapid assembly of nanomaterials and organics. *Acc. Chem. Res.* **2014**, *47*, 1338–1348. [CrossRef] [PubMed]
27. Rathi, A.K.; Gawande, M.B.; Zboril, R.; Varma, R.S. Microwave-assisted synthesis–catalytic applications in aqueous media. *Coord. Chem. Rev.* **2015**, *291*, 68–94. [CrossRef]
28. Ahmed, S.; Ahmad, M.; Swami, B.L.; Ikram, S. A review on plants extract mediated synthesis of silver nanoparticles for antimicrobial applications: A green expertise. *J. Adv. Res.* **2016**, *7*, 17–28. [CrossRef] [PubMed]
29. Sawai, J. Quantitative evaluation of antibacterial activities of metallic oxide powders (ZnO, MgO and CaO) by conductimetric assay. *J. Microbiol. Methods* **2003**, *54*, 177–182. [CrossRef]
30. Khan, J.; Ilyas, S.; Akram, B.; Ahmad, K.; Hafeez, M.; Siddiq, M.; Ashraf, M.A. Zno/NiO coated multi-walled carbon nanotubes for textile dyes degradation. *Arab. J. Chem.* **2018**, *11*, 880–896. [CrossRef]
31. Khan, J.; Siddiq, M.; Akram, B.; Ashraf, M.A. In-situ synthesis of CuO nanoparticles in P(NIPAM-co-AAA) microgel, structural characterization, catalytic and biological applications. *Arab. J. Chem.* **2018**, *11*, 897–909. [CrossRef]
32. Wojnarowicz, J.; Chudoba, T.; Lojkowski, W. A Review of Microwave Synthesis of Zinc Oxide Nanomaterials: Reactants, Process Parameters and Morphologies. *Nanomaterials* **2020**, *10*, 1086. [CrossRef] [PubMed]
33. Chandrasekhar, P.; Mukhopadhyay, A.; Savitha, G.; Moorthy, J.N. Remarkably selective and enantiodifferentiating sensing of histidine by a fluorescent homochiral Zn-MOF based on pyrene-tetralactic acid. *Chem Sci* **2016**, *7*, 3085–3091. [CrossRef] [PubMed]
34. Du, Y.; Dong, N.; Zhang, M.; Zhu, K.; Na, R.; Zhang, S.; Sun, N.; Wang, G.; Wang, J. Covalent functionalization of graphene oxide with porphyrin and porphyrin incorporated polymers for optical limiting. *Phys. Chem. Chem. Phys.* **2017**, *19*, 2252–2260. [CrossRef]
35. Akram, B.; Ahmad, K.; Khan, J.; Khan, B.A.; Akhtar, J. Low-temperature solution-phase route to sub-10 nm titanium oxide nanocrystals having super-enhanced photoreactivity. *New J. Chem.* **2018**, *42*, 10947–10952. [CrossRef]
36. Lange, B.M.; Croteau, R. Genetic engineering of essential oil production in mint. *Curr. Opin. Plant Biol.* **1999**, *2*, 139–144. [CrossRef] [PubMed]
37. Andro, A.R.; Atofani, D.; Boz, I.; Zamfirache, M.; Burzo, I.; Toma, C. Studies concerning the histo-anatomy and biochemistry of *Mentha longifolia* (L.) Huds. during vegetative phenophase. *An. Stiintifice Ale Univ. Al. I. Cuza Din Iasi* **2011**, *57*, 25.
38. Ertaş, A.; Gören, A.C.; Haşimi, N.; Tolan, V.; Kolak, U. Evaluation of Antioxidant, Cholinesterase Inhibitory and Antimicrobial Properties of Mentha longifolia subsp. noeana and Its Secondary Metabolites. *Rec. Nat. Prod.* **2015**, *9*, 105–115.
39. Khalid, A.; Ahmad, P.; Alharthi, A.I.; Muhammad, S.; Khandaker, M.U.; Faruque, M.R.I.; Khan, A.; Din, I.U.; Alotaibi, M.A.; Alzimami, K. Enhanced Optical and Antibacterial Activity of Hydrothermally Synthesized Cobalt-Doped Zinc Oxide Cylindrical Microcrystals. *Materials* **2021**, *14*, 3223. [CrossRef]
40. Khalid, A.; Ahmad, P.; Alharthi, A.I.; Muhammad, S.; Khandaker, M.U.; Rehman, M.; Faruque, M.R.I.; Din, I.U.; Alotaibi, M.A.; Alzimami, K. Structural, Optical and Antibacterial Efficacy of Pure and Zinc-Doped Copper Oxide against Pathogenic Bacteria. *Nanomaterials* **2021**, *11*, 451. [CrossRef]
41. Meek, S.T.; Greathouse, J.A.; Allendorf, M.D. Metal-organic frameworks: A rapidly growing class of versatile nanoporous materials. *Adv. Mater.* **2011**, *23*, 249–267. [CrossRef]
42. Han, X.; Yang, S.; Schröder, M. Porous metal–organic frameworks as emerging sorbents for clean air. *Nat. Rev. Chem.* **2019**, *3*, 108–118. [CrossRef]
43. Della Rocca, J.; Liu, D.; Lin, W. Nanoscale Metal Organic Frameworks for Biomedical Imaging and Drug Delivery. *Acc. Chem. Res.* **2011**, *44*, 957–968. [CrossRef]

44. Saeed, W.; Abbasi, Z.; Majeed, S.; Shahzad, S.A.; Khan, A.F.; Shaikh, A.J. An insight into the binding behavior of graphene oxide and noble metal nanoparticles. *J. Appl. Phys.* **2021**, *129*, 125302. [CrossRef]
45. Razzaq, Z.; Khalid, A.; Ahmad, P.; Farooq, M.; Khandaker, M.U.; Sulieman, A.; Rehman, I.U.; Shakeel, S.; Khan, A. Photocatalytic and Antibacterial Potency of Titanium Dioxide Nanoparticles: A Cost-Effective and Environmentally Friendly Media for Treatment of Air and Wastewater. *Catalysts* **2021**, *11*, 709. [CrossRef]
46. Mehta, S.S.; Nadargi, D.Y.; Tamboli, M.S.; Alshahrani, T.; Minnam Reddy, V.R.; Kim, E.S.; Mulla, I.S.; Park, C.; Suryavanshi, S.S. RGO/WO3 hierarchical architectures for improved H2S sensing and highly efficient solar-driving photo-degradation of RhB dye. *Sci. Rep.* **2021**, *11*, 5023. [CrossRef] [PubMed]
47. Singh, N.; Prakash, J.; Misra, M.; Sharma, A.; Gupta, R.K. Dual Functional Ta-Doped Electrospun TiO2 Nanofibers with Enhanced Photocatalysis and SERS Detection for Organic Compounds. *ACS Appl. Mater. Interfaces* **2017**, *9*, 28495–28507. [CrossRef]
48. Balasubramaniam, B.; Singh, N.; Kar, P.; Tyagi, A.; Prakash, J.; Gupta, R.K. Engineering of transition metal dichalcogenide-based 2D nanomaterials through doping for environmental applications. *Mol. Syst. Des. Eng.* **2019**, *4*, 804–827. [CrossRef]
49. Kar, P.; Jain, P.; Kumar, V.; Gupta, R.K. Interfacial engineering of Fe2O3@BOC heterojunction for efficient detoxification of toxic metal and dye under visible light illumination. *J. Environ. Chem. Eng.* **2019**, *7*, 102843. [CrossRef]
50. Kar, P.; Shukla, K.; Jain, P.; Sathiyan, G.; Gupta, R.K. Semiconductor based photocatalysts for detoxification of emerging pharmaceutical pollutants from aquatic systems: A critical review. *Nano Mater. Sci.* **2021**, *3*, 25–46. [CrossRef]
51. Hafeez, M.; Afyaz, S.; Khalid, A.; Ahmad, P.; Khandaker, M.U.; Sahibzada, M.U.K.; Ahmad, I.; Khan, J.; Alhumaydhi, F.A.; Emran, T.B. Synthesis of cobalt and sulphur doped titanium dioxide photocatalysts for environmental applications. *J. King Saud Univ.-Sci.* **2022**, *34*, 102028. [CrossRef]
52. Khalid, A.; Ahmad, P.; Khan, A.; Khandaker, M.U.; Kebaili, I.; Alam, M.M.; Din, I.U.; Muhammad, S.; Razzaq, Z.; Rehman, I.U.; et al. Cytotoxic and Photocatalytic Studies of Hexagonal Boron Nitride Nanotubes: A potential Candidate for Wastewater and Air Treatment. *RSC Adv.* **2022**, *12*, 6592–6600. [CrossRef]
53. Vanathi, P.; Rajiv, P.; Narendhran, S.; Rajeshwari, S.; Rahman, P.K.; Venckatesh, R. Biosynthesis and characterization of phyto mediated zinc oxide nanoparticles: A green chemistry approach. *Mater. Lett.* **2014**, *134*, 13–15. [CrossRef]
54. Ramesh, M.; Anbuvannan, M.; Viruthagiri, G. Green synthesis of ZnO nanoparticles using Solanum nigrum leaf extract and their antibacterial activity. *Spectrochim. Acta Part A Mol. Biomol. Spectrosc.* **2015**, *136*, 864–870. [CrossRef] [PubMed]
55. Kuznetsov, M.; Mafina, M.-K.; Belousova, O.; Vakin, N.; Shchipakin, S.Y.; Morozov, I.G. Catalytically active magnetic nanoparticles in the Cu-O system. *Inorg. Mater.* **2015**, *51*, 307–318. [CrossRef]
56. Padalia, H.; Baluja, S.; Chanda, S. Effect of pH on size and antibacterial activity of Salvadora oleoides leaf extract-mediated synthesis of zinc oxide nanoparticles. *Bionanoscience* **2017**, *7*, 40–49. [CrossRef]
57. Ullah, A.; Munir, S.; Badshah, S.L.; Khan, N.; Ghani, L.; Poulson, B.G.; Emwas, A.-H.; Jaremko, M. Important flavonoids and their role as a therapeutic agent. *Molecules* **2020**, *25*, 5243. [CrossRef]
58. Saravanan, R.; Karthikeyan, S.; Gupta, V.; Sekaran, G.; Narayanan, V.; Stephen, A. Enhanced photocatalytic activity of ZnO/CuO nanocomposite for the degradation of textile dye on visible light illumination. *Mater. Sci. Eng. C* **2013**, *33*, 91–98. [CrossRef]
59. Naika, H.R.; Lingaraju, K.; Manjunath, K.; Kumar, D.; Nagaraju, G.; Suresh, D.; Nagabhushana, H. Green synthesis of CuO nanoparticles using Gloriosa superba L. extract and their antibacterial activity. *J. Taibah Univ. Sci.* **2015**, *9*, 7–12. [CrossRef]
60. Patle, S.; Kumar, P. Decision making approach to prefer route repair technique in AODV routing protocol of MANET. *Int. J. Res. Eng. Technol* **2015**, *4*, 9–16.
61. Chen, C.; Yu, B.; Liu, P.; Liu, J.; Wang, L. Investigation of nano-sized ZnO particles fabricated by various synthesis routes. *J. Ceram. Process. Res.* **2011**, *12*, 420–425.
62. Hanawalt, J.D.; Rinn, H.W.; Frevel, L.K. Chemical Analysis by X-Ray Diffraction. *Ind. Eng. Chem. Anal. Ed.* **1938**, *10*, 457–512. [CrossRef]
63. Sundrarajan, M.; Ambika, S.; Bharathi, K. Plant-extract mediated synthesis of ZnO nanoparticles using Pongamia pinnata and their activity against pathogenic bacteria. *Adv. Powder Technol.* **2015**, *26*, 1294–1299. [CrossRef]
64. Widiarti, N.; Sae, J.; Wahyuni, S. Synthesis CuO-ZnO nanocomposite and its application as an antibacterial agent. In Proceedings of the IOP Conference Series: Materials Science and Engineering, 2017; IOP Publishing: Bristol, UK, 2017; p. 012036.
65. Das, D.; Nath, B.C.; Phukon, P.; Dolui, S.K. Synthesis and evaluation of antioxidant and antibacterial behavior of CuO nanoparticles. *Colloids Surf. B Biointerfaces* **2013**, *101*, 430–433. [CrossRef] [PubMed]
66. Gawade, V.; Gavade, N.; Shinde, H.; Babar, S.; Kadam, A.; Garadkar, K. Green synthesis of ZnO nanoparticles by using Calotropis procera leaves for the photodegradation of methyl orange. *J. Mater. Sci. Mater. Electron.* **2017**, *28*, 14033–14039. [CrossRef]
67. Barzegar, M.; Habibi-Yangjeh, A.; Behboudnia, M. Ultrasonic-assisted preparation and characterization of CdS nanoparticles in the presence of a halide-free and low-cost ionic liquid and photocatalytic activity. *J. Phys. Chem. Solids* **2010**, *71*, 1393–1397. [CrossRef]
68. Dai, D.; Wang, L.; Xiao, N.; Li, S.; Xu, H.; Liu, S.; Xu, B.; Lv, D.; Gao, Y.; Song, W.; et al. In-situ synthesis of Ni2P co-catalyst decorated Zn0.5Cd0.5S nanorods for high-quantum-yield photocatalytic hydrogen production under visible light irradiation. *Appl. Catal. B Environ.* **2018**, *233*, 194–201. [CrossRef]
69. Wali, L.A.; Alwan, A.M.; Dheyab, A.B.; Hashim, D.A. Excellent fabrication of Pd-Ag NPs/PSi photocatalyst based on bimetallic nanoparticles for improving methylene blue photocatalytic degradation. *Optik* **2019**, *179*, 708–717. [CrossRef]

70. Ravichandran, K.; Mohan, R.; Sakthivel, B.; Varadharajaperumal, S.; Devendran, P.; Alagesan, T.; Pandian, K. Enhancing the photocatalytic efficiency of sprayed ZnO thin films through double doping (Sn+F) and annealing under different ambiences. *Appl. Surf. Sci.* **2014**, *321*, 310–317. [CrossRef]
71. Wu, X.; Wen, L.; Lv, K.; Deng, K.; Tang, D.; Ye, H.; Du, D.; Liu, S.; Li, M. Fabrication of ZnO/graphene flake-like photocatalyst with enhanced photoreactivity. *Appl. Surf. Sci.* **2015**, *358*, 130–136. [CrossRef]